JACS Au
AN OPEN ACCESS JOURNAL OF THE AMERICAN CHEMICAL SOCIETY

pubs.acs.org/jacsau
Article

Robust Accessibility of Addressable Sites in Defective DNA Origami

Zheze Dai, Xiaodong Xie, Xiaoliang Chen, Hui Lv, Yao Xie, Yongjun Liu, Fei Wang, Mingqiang Li, Chunhai Fan,* and Qian Li*

Cite This: JACS Au 2025, 5, 2237−2245
Read Online

ACCESS | Metrics & More | Article Recommendations | Supporting Information

ABSTRACT: Owing to its unique programmability and addressability, DNA origami-based nanofabrication has been widely utilized in fields such as nanomedicine and nanophotonics. The accessibility of addressable sites on DNA origami structures is crucial for their use as nanofabrication platforms. In this study, we systematically investigated the impact of structural defects on accessibility using a classic six-helix bundle (6HB) DNA origami and two variants with subsets of DNA staple strands deleted, introducing programmable defects in 6HB nanostructures. DNA point accumulation for imaging in nanoscale topography super-resolution microscopy was employed to monitor hybridization and dehybridization at each addressable site and analyze corresponding localizations and kinetics. Statistical analysis revealed that addressable sites on 6HB nanostructures retained significant accessibility robustness despite structural defects, which was further supported by molecular dynamics simulations. These results provide valuable insights into the design principles and applications of DNA origami.

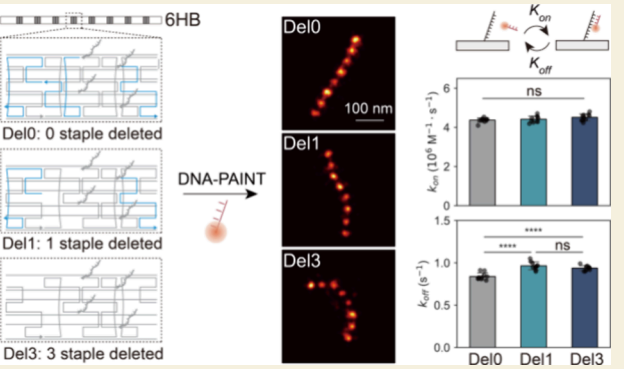

KEYWORDS: *DNA origami, DNA nanotechnology, addressable sites, accessibility, DNA-PAINT*

INTRODUCTION

Leveraging the predictable base-pairing rules of DNA molecules, structural DNA nanotechnology has empowered the creation of intricately customized structures with nucleotide-level precision since the 1980s.[1−4] Over the years, numerous successful methods have been developed to fabricate DNA nanostructures of almost any arbitrary geometry.[5−9] Among them, the DNA origami technique,[6] pioneered by Rothemund in 2006, uses hundreds of short DNA oligonucleotides (staples) to fold a long single-stranded scaffold into a predefined shape via a one-pot self-assembly process. By providing precise spatial control over the arrangement of functional moieties, such as molecules and particles, DNA origami has emerged as a powerful platform for nanofabrication.[10−12]

DNA origami-based nanofabrication offers exceptional programmability and has been extensively utilized in various fields, such as nanophotonics,[13,14] nanomedicine,[15−17] nanorobots,[18,19] and artificial enzymatic reaction networks.[20,21] Its functionality critically relies on postassembly or direct chemical modification of functional entities on addressable sites, typically single-stranded DNA (ssDNA) tethers on the DNA origami surface.[22] Therefore, to efficiently functionalize DNA origami, exploration of the parameters that affect the accessibility of these addressable sites is essential, particularly for the postassembly DNA−DNA hybridization method. Structural defects, such as missing staples, could alter the mechanical rigidity and thermal stability of DNA origami and thus potentially impact the hybridization dynamics at addressable sites.[23] However, whether such structural perturbations directly translate into functional impairment of accessibility remains to be systematically explored.

Atomic force microscopy (AFM) and electron microscopy (EM) provide detailed structural and morphological information on DNA origami nanostructures[7] but cannot assess the accessibility of addressable sites on these nanostructures. Alternatively, DNA point accumulation for imaging in nanoscale topography (DNA-PAINT)[24,25] allows for precise characterization of addressable sites on DNA origami. Previous studies have explored ssDNA accessibility on both two-dimensional[26,27] and three-dimensional[28] DNA origami structures, revealing site location dependency and structural correlations. For instance, due to steric hindrance and positional differences, central binding domains in rectangular DNA origami typically exhibit higher accessibility than edge sites.[26] Despite these advances, a quantitative understanding of

Received: February 20, 2025
Revised: March 27, 2025
Accepted: March 28, 2025
Published: May 13, 2025

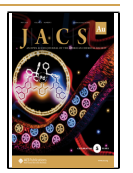

https://doi.org/10.1021/jacsau.5c00206
JACS Au 2025, 5, 2237−2245

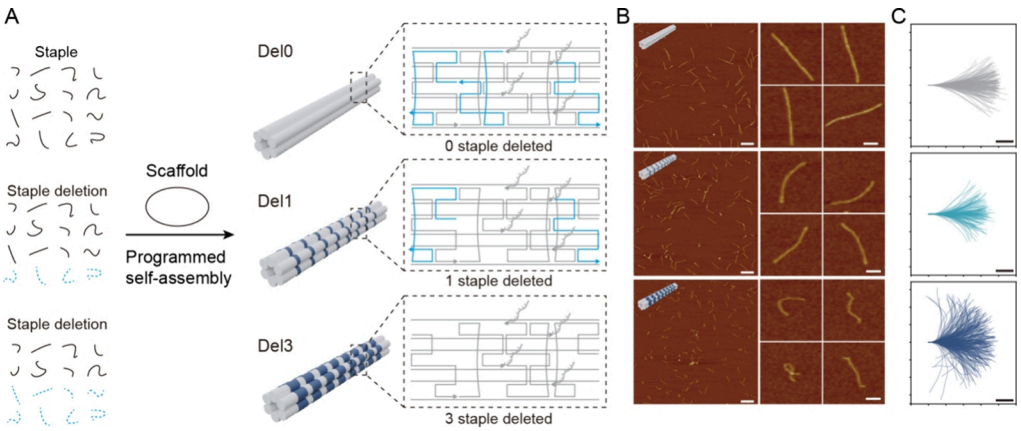

Figure 1. Overview of the design and self-assembly of 6HB DNA origami with three levels of defects. (A) Schematic of the self-assembly of 6HB origami with varying levels of defects. Del0 represents a defect-free 6HB with no staple strands removed from a single addressable site; Del1 and Del3 have one and three staple strands removed from a single addressable site, respectively. (B) Representative AFM images of 6HB DNA origami with varying defects. Left: wide-field AFM images. Scale bars: 500 nm. Right: representative AFM images of individual structures. Scale bars: 100 nm. (C) Contour statistics of 6HB origami with varying defects. Contours from over 100 representative monomers for each design are aligned with initial tangents horizontally. Scale bars: 100 nm.

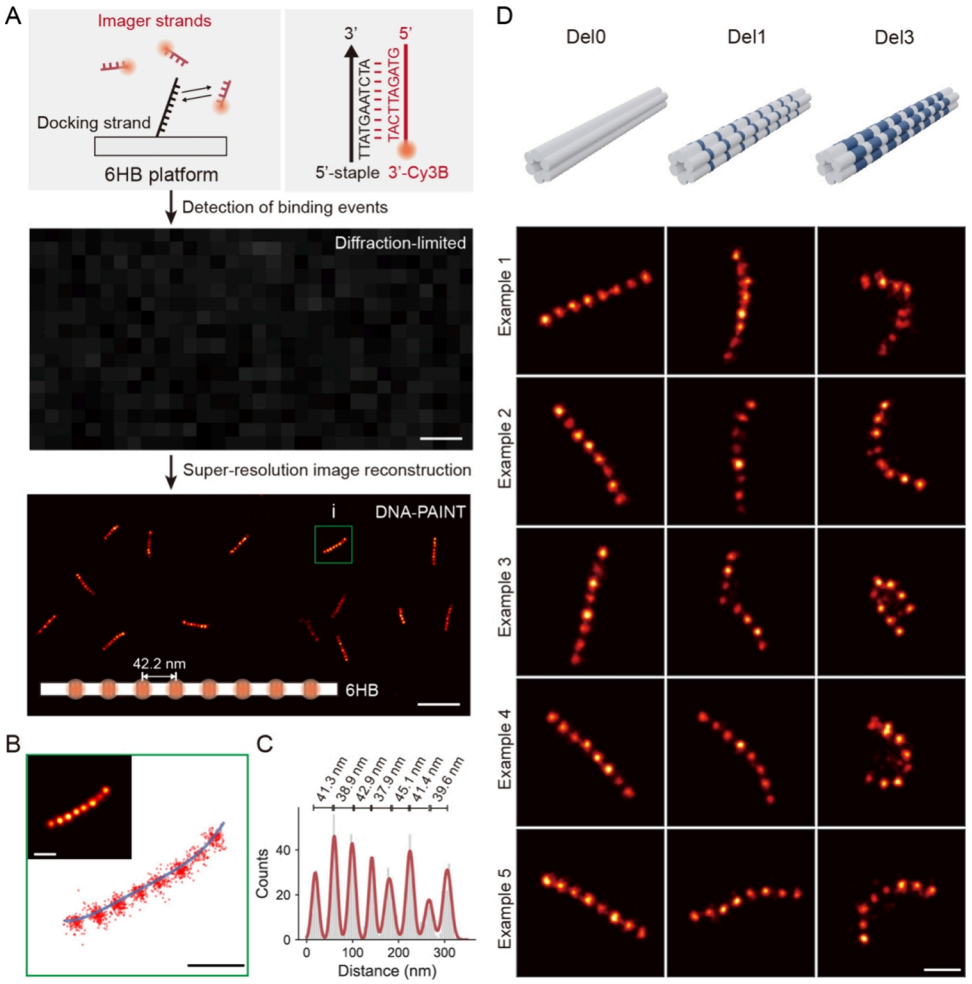

Figure 2. Super-resolution imaging of 6HB origami with three defect levels. (A) Workflow of super-resolution DNA-PAINT imaging of the 6HB. Up: sequence design for DNA-PAINT super-resolution imaging experiments. Middle: a diffraction-limited image of 6HB structures. Scale bar: 500 nm. Bottom: reconstructed super-resolution DNA-PAINT image of the 6HB structure. Scale bar: 500 nm. (B) Localization of DNA-PAINT binding events and extracted monomer contour from the green boxed region in panel (C). Scale bar: 100 nm. (C) Histogram of localization counts along the contour of a single 6HB and one-dimensional Gaussian fitting along its contour. (D) Visualization of binding domains in 6HBs with three levels of defects. Representative DNA-PAINT images of Del0 (defect-free), Del1, and Del3. Scale bar: 100 nm.

https://doi.org/10.1021/jacsau.5c00206
JACS Au 2025, 5, 2237−2245

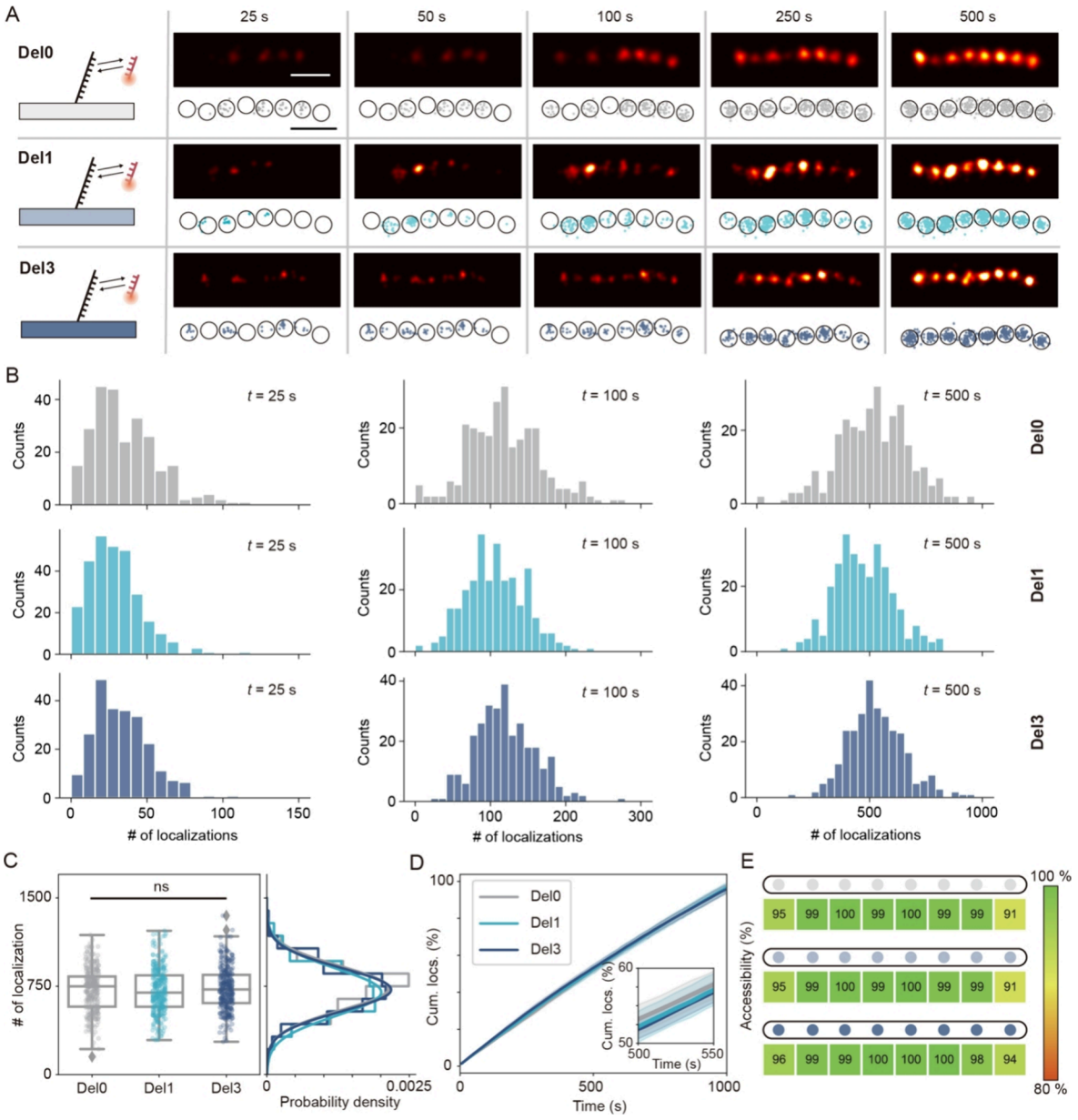

Figure 3. Localization analysis of accessibility in 6HB DNA origami with varying levels of defects. (A) Time-lapse imaging of DNA binding events on a single 6HB. Representative DNA-PAINT images (top) and specific binding events (bottom) at addressable sites for Del0, Del1, and Del3 at increasing acquisition times (25−500 s). Scale bars: 100 nm. (B) Distribution of localizations over time. Histograms show localizations detected at 25, 100, and 500 s for Del0, Del1, and Del3. (C) Quantitative comparison of localizations of Del0, Del1, and Del3 within 500 s. Box plots (left) display localization distributions for 300 independent structures of each design. Probability density plots (right) illustrate similar distributions despite increased defects. (D) Cumulative localizations as a function of time over 1000 s (N = 6). The inset shows a magnified view of an intermediate time point. (E) Accessibility heatmap for eight addressable sites of Del0, Del1, and Del3.

how structural defects specifically affect ssDNA accessibility remains limited.

Here, we employed the classic six-helix bundle (6HB) DNA origami[29] and its two variants with deleted subsets of required DNA staple strands as a model system to systematically analyze the impact of structural defects on the accessibility of addressable sites. By combining DNA-PAINT super-resolution microscopy and molecular dynamics simulations, we quantitatively evaluated accessibility across 6HB structures with varying defect designs. Our results demonstrate that the accessibility of addressable sites on DNA origami remains largely unaffected despite structural perturbations caused by the removal of staple strands.

RESULTS AND DISCUSSION

Design and Assembly of 6HB DNA Origami with Different Levels of Defect

We employed the classic 6HB DNA origami, featuring a slender honeycomb lattice geometry, as the model system.

Previous studies have reported the impact of defects on the geometry and mechanical performance of 6HB origami, making it an ideal framework for our investigation.[30,31] Using the caDNAno software,[32] we engineered two 6HB structures with varying levels of defects (Figure 1A). The intact 6HB DNA origami structure has a total length of 400 nm, an inner diameter of 2 nm, and an outer diameter of 6 nm, with eight

https://doi.org/10.1021/jacsau.5c00206
JACS Au 2025, 5, 2237−2245

addressable sites evenly spaced along the structure, each 42.2 nm apart. At each addressable site, four protruding 11 nt ssDNA are available for subsequent accessibility evaluation (Figure 1A and Figures S1 and S2). These three distinct 6HB designs with varying defect levels were constructed through a one-step annealing process: (i) an intact 6HB DNA origami (Del0), without missing staple strands; (ii) a partially defective 6HB DNA origami (Del1), with one staple strand missing at a single addressable site; and (iii) a severely defective structure (Del3), with three staple strands missing at a single addressable site. Defects were uniformly introduced into the eight addressable sites distributed evenly along the 6HB. AFM imaging confirmed the successful folding of all defect-programmed 6HB structures (Figure 1B and Figures S3–S6). To further visualize the AFM characterization results, we aligned the contour lines of 6HB monomers at one end (Figure 1C), where increased contour fluctuations were observed with higher defect levels. These observations validate the successful fabrication of 6HB origami structures with three distinct defect states.

Super-Resolution Imaging of Defect-Engineered 6HB DNA Origami

In our DNA-PAINT imaging experiments, the four 11 nt ssDNA protruding from each addressable site of a single 6HB served as docking strands, while the complementary Cy3B-labeled 9 nt ssDNA acted as imager strands (Figure 2A). To ensure unbiased comparisons, DNA-PAINT data acquisition was conducted under identical experimental conditions for all three types of 6HB DNA origami (Del0, Del1, and Del3). The fluorescently labeled imager strands transiently and reversibly bind to the docking strands located on the eight addressable sites of each 6HB (Figure 2A). By localizing the detected single-molecule binding events, diffraction-limited images of the 6HB DNA origami were obtained, which were further processed using image reconstruction techniques to produce super-resolution DNA-PAINT images (Figure 2A).

To quantify accessibility at the level of individual addressable sites, we analyzed the spatial resolution of DNA-PAINT images. We counted the localized binding events from the super-resolution images of the 6HB to extract the contour of the individual 6HB (Figure 2B). The DNA-PAINT imaging resolution of the 6HB was calculated using the histogram of localization counts and one-dimensional Gaussian fitting along the contour line (Figure 2C). Super-resolution images of the 6HB with varying defect levels consistently revealed a clear pattern of eight distinct points (Figure 2D and Figures S7–S9). Notably, as structural defects increased, the contour fluctuations of the 6HB became more pronounced (Figure S10), consistent with AFM observations (Figure 1B). Although the inherent flexibility of the 6HB and defect-induced rigidity reduction caused significant structural bending, the reconstructed super-resolution images demonstrated exceptional spatial resolution. The cross-sectional histograms revealed that the averaged distances between two addressable sites for the three types of 6HB were approximately 42.2 ± 3.4, 41.7 ± 3.6, and 40.9 ± 4.4 nm (Figures S11 and S12), which closely matched the designed theoretical spacing of 42.2 nm. The full width at half-maximum (fwhm) resolution, determined by Gaussian fitting of the reconstructed images, was approximately 13.1 nm for all three types of 6HB (Figure S11c), indicating that structural defects did not significantly impact spatial resolution for the individual addressable site in DNA-PAINT experiments.

Accessibility of Defect-Engineered 6HBs

To quantify the accessibility of addressable sites at 6HBs, we applied a localization threshold to distinguish detectable sites and determined their absolute accessibility by statistically analyzing a large number of 6HB structures. Localizations generated by binding of the 9 nt imager strand to docking strands on 6HBs were used as a metric to measure the accessibility of addressable sites. An increase in localizations indicates more binding events of imager strands to the docking strands, providing a reliable quantitative assessment for addressable sites' accessibility within an individual 6HB DNA origami.

DNA-PAINT imaging results revealed that the eight addressable sites in one single 6HB could be clearly distinguished within 250 s at a constant imager concentration of 5 nM (Figure 3A and Figure S13). The localizations of the three 6HB variants were comparable over time (Figure 3B). Specifically, the observed average localizations for a single Del0, Del1, and Del3 within 500 s were 733 ± 187, 699 ± 200, and 720 ± 182, respectively (mean ± SD, n = 300), indicating minimal impact of defect on the accessibility of addressable sites (Figure 3C). To validate these findings, we analyzed the cumulative changes in localizations over time (Figure 3D) and found out that the localizations increased linearly with time for all three 6HB structures within 1000 s, with very similar growth rates. The comparable localizations and consistent cumulative changes of localizations over time for Del0, Del1, and Del3 clearly indicated that structural defects had minimal effect on the accessibility of addressable sites. A higher level of structural defects resulted in 6HB assembly failure and loss of addressable sites. As shown in Figure S14, the eight addressable sites in one single Del6 could not be distinguished by DNA-PAINT.

Next, we conducted absolute quantification of addressable sites' accessibility by analyzing the localization data of eight addressable sites in 300 6HB DNA origami and compared those of Del0, Del1, and Del3. For all three 6HB variants, over 85% of DNA origami exhibited complete sets of eight points in DNA-PAINT images (Figure S15). The accessibility of eight addressable sites showed no significant correlation with defects, though a slight position dependency was observed, with central regions exhibiting slightly higher accessibility than peripheral regions (Figure 3E and Figure S16).

Taken together, these results indicated that the accessibility of addressable sites is not significantly affected by structural defects in 6HBs, even when up to 14% of staples (24 out of 172 staples) were omitted from the self-assembly reaction mixtures.

This robust accessibility highlights the resilience of the addressable sites in DNA origami against structural perturbations.

Hybridization/Dehybridization Kinetics of Addressable Sites on Defect-Engineered 6HBs

To further elucidate the accessibility of addressable sites in 6HBs with varying defect levels, we conducted a comprehensive analysis of single-molecule binding kinetics. Binding kinetics were characterized by two key parameters: bright time (τ_b) and dark time (τ_d) (Figure 4A). Bright time (τ_b) represents the duration of hybridization between the imager strand and the extended staples on 6HBs, during which

https://doi.org/10.1021/jacsau.5c00206
JACS Au 2025, 5, 2237−2245

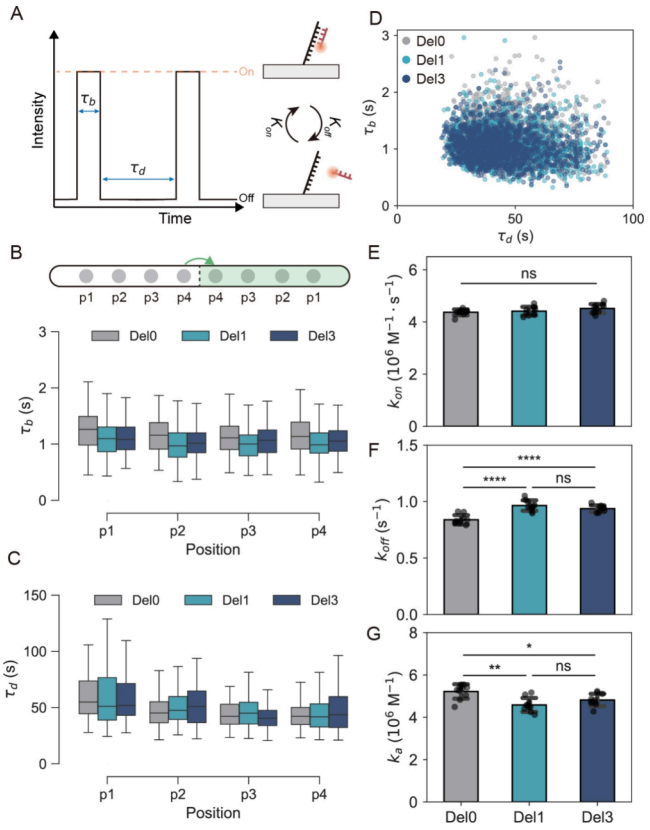

Figure 4. Hybridization kinetics at addressable sites on 6HBs with varying levels of defects. (A) Schematic of blinking-based detection of accessibility. τ_b and τ_d represent bright and dark times obtained from intensity−time trajectories, respectively. (B, C) Statistical analysis of mean bright and dark times for Del0, Del1, and Del3. 100 structures. Box plots indicate the 25th and 75th percentiles, with the median marked by a line within the box. (D) Scatter plots of τ_b and τ_d for Del0, Del1, and Del3 (N = 1500). (E) Constant of hybridization rate (k_{on}), (F) constant of dissociation rate (k_{off}), and (G) affinity constant ($k_a = k_{on}/k_{off}$) for hybridization at addressable sites in Del0, Del1, and Del3 (N = 10). ns, not significant; *$P \leq 0.05$, **$P \leq 0.01$,, ****$P \leq 0.0001$ by the two-tailed paired Student's t test.

fluorescence spots appear under total internal reflection fluorescence (TIRF) microscopy. This parameter reflects the stability of hybridization, influenced by intrinsic factors such as imager sequence and length.[33] In contrast, dark time (τ_d) corresponds to the interval when no hybridization occurs, reflecting the diffusion and hybridization dynamics of the imager, which are modulated by factors such as sequence, buffer conditions,[34] and particularly the concentration of imager strands.[35] Together, τ_b and τ_d provide detailed insights into addressable sites' accessibility of different defect-level 6HBs at the single-molecule level.

Due to the bilaterally symmetric design of 6HBs, addressable sites were categorized into four groups (p1, p2, p3, and p4), based on their relative positions to 6HB edges. The average bright times (τ_b) for 100 single 6HBs were identical for Del0, Del1, and Del3, indicating consistent binding durations between the imager strands and docking strands (Figure 4B and Figure S17). However, slight differences in average dark time (τ_d) were observed, with edge sites (p1 and p2) showing slightly longer dark times compared to central positions (p3 and p4) (Figure 4C and Figure S18). This observation suggests a mild spatial dependence in accessibility, with enhanced hybridization dynamics at central sites. These findings align with prior observations of accessibility variations in linear DNA nanostructures.[35] Scatter plot analyses of τ_b and τ_d for 1500 individual Del0, Del1, and Del3 revealed consistent hybridization/dehybridization kinetics regardless of defect levels (Figure 4B and Figure S19), indicating that structural defects have minimal impact on hybridization/dehybridization kinetics at addressable sites.

To assess whether photobleaching influences τ_b measurements, we conducted photobleaching experiments (Figure S20). The photobleaching rate of Cy3B fluorophores ($k_{photobleaching}$ = 0.3 s^{-1}) was significantly slower than the slowest dissociation rate measured for Del0 structures (k_{off} = 0.84 s^{-1}), confirming that dissociation dynamics dominated τ_b measurements, and photobleaching interference was negligible. Therefore, the photophysical properties of Cy3B fluorophores did not compromise the accuracy of hybridization kinetics. Notably, DNA-PAINT typically uses imager-docking strands of 9 or 10 nt with binding times shorter than 2 s.[35] Longer sequences of imager-docking strands increase binding strength and hybridization time, raising the risk of photobleaching and overestimation of k_{on}, which should be considered for the evaluation of addressable sites' accessibility.

The constants of binding rate (k_{on}) for Del0, Del1, and Del3 were calculated to be approximately 4.37 × 10^6, 4.41 × 10^6, and 4.51 × 10^6 $M^{-1}s^{-1}$, respectively, showing no significant dependence on defect levels (Figure 4E). Similarly, the constant of dissociation rate (k_{off}) was consistent, with average values of 0.84, 0.97, and 0.94 s^{-1} (Figure 4F), respectively. The affinity constant ($k_a = k_{on}/k_{off}$) also remained stable, averaging approximately 5.22 × 10^6, 4.59 × 10^6, and 4.82 × 10^6 M^{-1}, respectively (Figure 4G). These results further confirm that structural defects in the 6HB DNA origami do not significantly affect the accessibility of addressable sites. While k_{off} and k_a exhibit variations, the statistical analysis results indicate that these differences are not substantial enough to alter the overall accessibility of addressable sites. Specifically, the localization counts, binding kinetics, and temporal sampling dynamics remain comparable across three defect levels. Additionally, the observed variations in k_{off} and k_a fall within expected fluctuations due to the slight fluctuations in the experimental environment rather than a systematic disruption of functional accessibility.

Molecular Dynamics Simulation

To investigate why the defect levels of 6HBs do not impact the accessibility of addressable sites, molecular dynamics (MD) simulations were conducted (Figure 5). We first quantified the extent of thermodynamic fluctuations in Del0, Del1, and Del3 structures using root-mean-square fluctuation (RMSF), where higher RMSF values correspond to greater fluctuations and are directly correlated with the extent of structural defects. The MD results demonstrated that increasing the number of missing staples led to larger thermodynamic fluctuations, inducing greater overall instability of 6HBs (Figure 5A and Figure S21A). Further analysis revealed that the distribution of RMSF values across the extension single strands in different addressable sites showed only minor variations (Figure S21B–D), indicating that the impact of structural defects on thermodynamic fluctuations was not significantly position-dependent.

We then statistically analyzed the theoretical lengths of all 32 11 nt ssDNA protruding from eight addressable sites in Del0,

https://doi.org/10.1021/jacsau.5c00206
JACS Au 2025, 5, 2237−2245

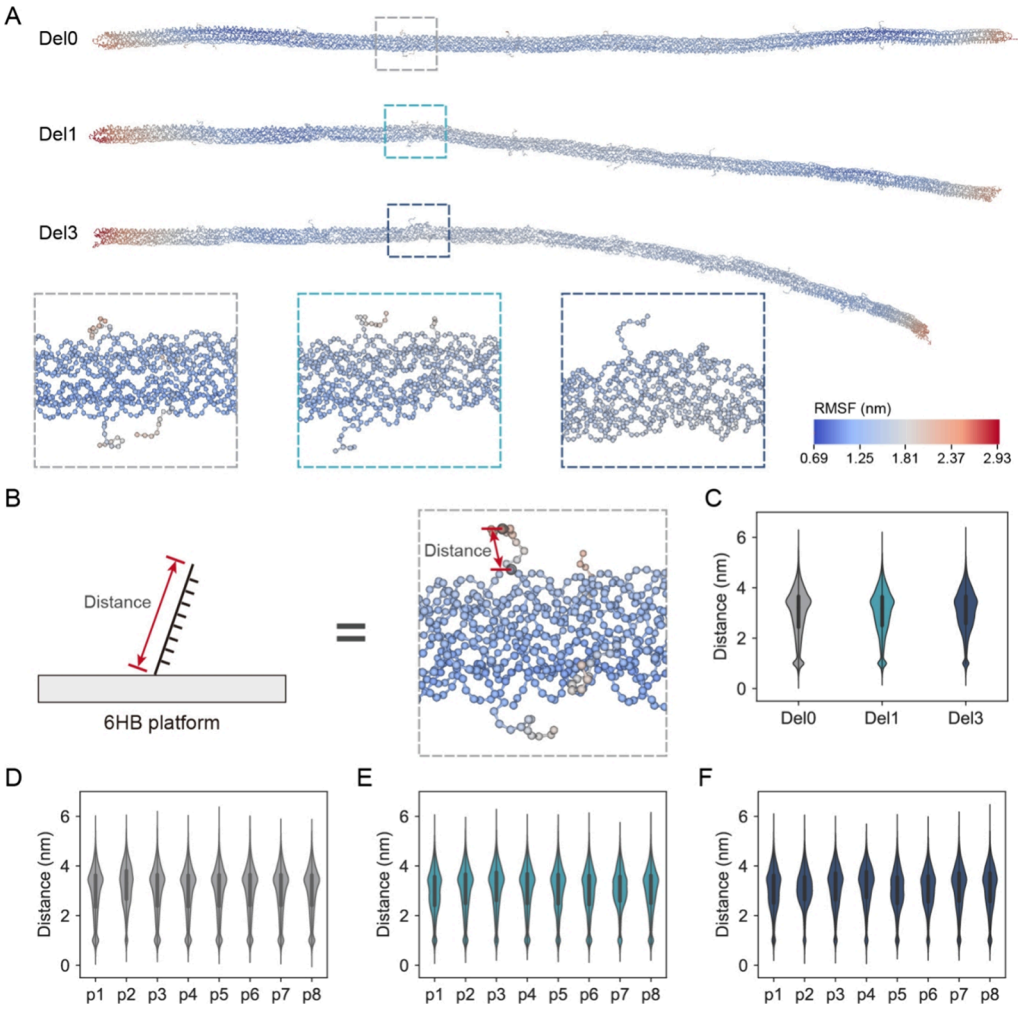

Figure 5. MD simulations of 6HB origami with varying defects. (A) Average structural models of Del0, Del1, and Del3 derived from MD simulations. (B) Schematic representation of theoretical length measurements for single extended staples at addressable sites of Del0, Del1, and Del3. Distances (D) are measured as the relative distance between the first and last nucleotide of each extended DNA strand. (C) Statistical distribution of theoretical lengths for all extended staples in Del0, Del1, and Del3. Mean lengths are 3.00 ± 0.96, 3.02 ± 0.91, and 3.08 ± 0.84 nm, respectively (mean ± SD). (D−F) Distribution of theoretical lengths for extended staples across eight addressable sites in Del0, Del1, and Del3.

Del1, and Del3 structures (Figure 5B) and found that the average lengths of these ssDNA were comparable (Figure 5C). These findings indicate that ssDNA flexibility remained largely unaffected by neighboring structural defects. Additionally, the distance distributions of all extended staples across eight addressable sites were similar (Figure 5D−F), further suggesting minimal position dependence of ssDNA flexibility.

The results confirm that, despite increased thermodynamic fluctuations in 6HB structures of a higher level of defects, the theoretical hybridization lengths of ssDNA at addressable sites do not undergo significant changes. This consistency ensures that the accessibility of addressable sites in Del0, Del1, and Del3 remains relatively uniform. These findings highlight the resilience of 6HB DNA origami, which can tolerate substantial mechanical and structural perturbations while maintaining the functional accessibility of addressable sites. This robustness underscores the potential of 6HB DNA origami for applications requiring precise molecular accessibility under challenging conditions.

CONCLUSIONS

The accessibility of addressable sites on DNA origami structures is crucial for their functionalization. The exploration of the accessibility of addressable sites is essential for ensuring the functionality, reliability, and applicability of DNA origami structures. We systematically investigated the impact of structural defects on the accessibility of eight addressable sites within 6HB DNA origami using DNA-PAINT super-resolution microscopy and MD simulations. Structural defects were introduced into 6HBs by deleting one and three staples in each addressable site. DNA-PAINT images of 6HBs with varying defect levels consistently revealed a clear pattern of eight distinct points for predesigned eight addressable sites, with comparable spatial resolution. Quantitative analyses revealed no significant differences in localizations, binding kinetics, or temporal sampling dynamics between intact designs (Del0) and those with moderate (Del1) or severe (Del3) defects. Detailed kinetic analyses showed that key parameters, including bright time (τ_b), dark time (τ_d), hybridization rate constant (k_{on}), and dissociation rate constant (k_{off}), were uniformly distributed across all defect levels, highlighting the intrinsic stability of addressable sites.

https://doi.org/10.1021/jacsau.5c00206
JACS Au 2025, 5, 2237−2245

MD simulations supported these observations, revealing that while structural defects increased thermodynamic fluctuations, they did not compromise the accessibility or functional integrity of the extended staples at addressable sites. These results demonstrate the exceptional structural integrity and functional reliability of 6HB DNA origami nanostructures, even under significant structural and mechanical perturbations. The higher accessibility observed in the central region is likely due to differences in staple incorporation efficiency rather than spatial positioning effects. MD simulations (Figure 5) indicate that the flexibility of protruding strands is unaffected by their location, implying that structural factors do not drive the observed accessibility differences. Instead, staple strands at the periphery are more prone to loss during DNA origami assembly or purification due to the lack of neighboring duplex support and base stacking interactions. This remarkable robustness of the addressable sites' accessibility of defective 6HB DNA origami provides valuable insights for the design and applications of DNA origami and contributes to the fundamental understanding of how DNA nanostructures behave at the molecular level.

DNA origami nanostructures have been extensively engineered as programmable platforms for targeted drug delivery,[15] biosensing,[3,10] and molecular diagnostics,[16,17] where functional integrity under operational conditions is critical. Our findings reveal that functional sites' accessibility exhibits remarkable insensitivity to structural imperfections (e.g., up to 14% staples omitted in 6HB) arising during self-assembly or under physiological conditions. This defect tolerance validates the reliability of DNA origami as scaffolds in maintaining molecular recognition fidelity, which is a critical prerequisite for their utilization in biomedical applications, where environmental perturbations necessitate function robustness. We envision that the utility and resilience of DNA origami could be further enhanced by exploration on the structure and functionality in various environmental conditions.

■ ASSOCIATED CONTENT

Supporting Information

The Supporting Information is available free of charge at https://pubs.acs.org/doi/10.1021/jacsau.5c00206.

Materials and reagents, synthesis of the defect-engineered 6HBs, AFM and DNA-PAINT characterization and analysis, statistical distributions of the accessibility of the 6HB origami, coarse-grained modeling, and calculation of DNA origami (PDF)

■ AUTHOR INFORMATION

Corresponding Authors

Chunhai Fan − *State Key Laboratory of Synergistic Chem-Bio Synthesis, School of Chemistry and Chemical Engineering, New Cornerstone Science Laboratory, Frontiers Science Center for Transformative Molecules, National Center for Translational Medicine, Shanghai Jiao Tong University, Shanghai 200240, China; Institute of Molecular Medicine, Shanghai Key Laboratory for Nucleic Acids Chemistry and Nanomedicine, Renji Hospital, School of Medicine, Shanghai Jiao Tong University, Shanghai 200127, China;* orcid.org/0000-0002-7171-7338; Email: fanchunhai@sjtu.edu.cn

Qian Li − *State Key Laboratory of Synergistic Chem-Bio Synthesis, School of Chemistry and Chemical Engineering, New Cornerstone Science Laboratory, Frontiers Science Center for Transformative Molecules, National Center for Translational Medicine, Shanghai Jiao Tong University, Shanghai 200240, China*; Email: liqian2018@sjtu.edu.cn

Authors

Zheze Dai − *State Key Laboratory of Synergistic Chem-Bio Synthesis, School of Chemistry and Chemical Engineering, New Cornerstone Science Laboratory, Frontiers Science Center for Transformative Molecules, National Center for Translational Medicine, Shanghai Jiao Tong University, Shanghai 200240, China*

Xiaodong Xie − *State Key Laboratory of Synergistic Chem-Bio Synthesis, School of Chemistry and Chemical Engineering, New Cornerstone Science Laboratory, Frontiers Science Center for Transformative Molecules, National Center for Translational Medicine, Shanghai Jiao Tong University, Shanghai 200240, China*

Xiaoliang Chen − *State Key Laboratory of Synergistic Chem-Bio Synthesis, School of Chemistry and Chemical Engineering, New Cornerstone Science Laboratory, Frontiers Science Center for Transformative Molecules, National Center for Translational Medicine, Shanghai Jiao Tong University, Shanghai 200240, China*

Hui Lv − *State Key Laboratory of Synergistic Chem-Bio Synthesis, School of Chemistry and Chemical Engineering, New Cornerstone Science Laboratory, Frontiers Science Center for Transformative Molecules, National Center for Translational Medicine, Shanghai Jiao Tong University, Shanghai 200240, China*

Yao Xie − *State Key Laboratory of Synergistic Chem-Bio Synthesis, School of Chemistry and Chemical Engineering, New Cornerstone Science Laboratory, Frontiers Science Center for Transformative Molecules, National Center for Translational Medicine, Shanghai Jiao Tong University, Shanghai 200240, China*

Yongjun Liu − *State Key Laboratory of Synergistic Chem-Bio Synthesis, School of Chemistry and Chemical Engineering, New Cornerstone Science Laboratory, Frontiers Science Center for Transformative Molecules, National Center for Translational Medicine, Shanghai Jiao Tong University, Shanghai 200240, China*

Fei Wang − *State Key Laboratory of Synergistic Chem-Bio Synthesis, School of Chemistry and Chemical Engineering, New Cornerstone Science Laboratory, Frontiers Science Center for Transformative Molecules, National Center for Translational Medicine, Shanghai Jiao Tong University, Shanghai 200240, China;* orcid.org/0000-0003-3948-6899

Mingqiang Li − *State Key Laboratory of Synergistic Chem-Bio Synthesis, School of Chemistry and Chemical Engineering, New Cornerstone Science Laboratory, Frontiers Science Center for Transformative Molecules, National Center for Translational Medicine, Shanghai Jiao Tong University, Shanghai 200240, China;* orcid.org/0000-0001-9854-2251

Complete contact information is available at: https://pubs.acs.org/10.1021/jacsau.5c00206

Author Contributions

All authors have given approval to the final version of the manuscript. CRediT: **Zheze Dai** data curation, formal analysis,

https://doi.org/10.1021/jacsau.5c00206
JACS Au 2025, 5, 2237−2245

investigation, visualization, writing - original draft, writing - review & editing; **Xiaodong Xie** data curation, formal analysis, investigation, validation, visualization; **Xiaoliang Chen** formal analysis, funding acquisition, methodology, project administration, visualization, writing - original draft, writing - review & editing; **Hui Lv** formal analysis, methodology, project administration, validation, visualization; **Yao Xie** data curation, investigation, validation; **Yongjun Liu** methodology, resources, software; **Fei Wang** funding acquisition, methodology, resources; **Mingqiang Li** formal analysis, funding acquisition, methodology, resources, software; **Chunhai Fan** conceptualization, formal analysis, funding acquisition, resources, supervision, writing - review & editing; **Qian Li** conceptualization, formal analysis, funding acquisition, methodology, resources, supervision, visualization, writing - original draft, writing - review & editing.

Notes

The authors declare no competing financial interest.

■ ACKNOWLEDGMENTS

This work was financially supported by the National Key R&D Program of China (2024YFF1206300), the National Natural Science Foundation of China (T2188102 and 22322704), Shanghai Pilot Program for Basic Research-Shanghai Jiao Tong University (21TQ1400222), Startup Fund for Young Faculty at SJTU (AF3250015), Shanghai Science and Technology Innovation Action Plan (24ZR1433100), Shanghai Municipal Science and Technology Major Project, the New Cornerstone Science Foundation, and K. C. Wong Education Foundation.

■ REFERENCES

(1) Dey, S.; Fan, C. H.; Gothelf, K.; Li, J.; Lin, C. X.; Liu, L. F.; Liu, N.; Nijenhuis, M. A. D.; Saccà, B.; Simmel, F. C.; et al. DNA origami. *Nat. Rev. Methods Primers* **2021**, *1* (1), 13.
(2) Hong, F.; Zhang, F.; Liu, Y.; Yan, H. DNA Origami: Scaffolds for Creating Higher Order Structures. *Chem. Rev.* **2017**, *117* (20), 12584−12640.
(3) Seeman, N. C.; Sleiman, H. F. DNA nanotechnology. *Nat. Rev. Mater.* **2017**, *3* (1), 17068.
(4) Ramezani, H.; Dietz, H. Building machines with DNA molecules. *Nat. Rev. Genet.* **2020**, *21* (1), 5−26.
(5) Seeman, N. C. NUCLEIC-ACID JUNCTIONS AND LATTICES. *J. Theor. Biol.* **1982**, *99* (2), 237−247.
(6) Rothemund, P. W. K. Folding DNA to create nanoscale shapes and patterns. *Nature* **2006**, *440* (7082), 297−302.
(7) Wei, B.; Dai, M. J.; Yin, P. Complex shapes self-assembled from single-stranded DNA tiles. *Nature* **2012**, *485* (7400), 623−626.
(8) Dietz, H.; Douglas, S. M.; Shih, W. M. Folding DNA into Twisted and Curved Nanoscale Shapes. *Science* **2009**, *325* (5941), 725−730.
(9) Veneziano, R.; Ratanalert, S.; Zhang, K.; Zhang, F.; Yan, H.; Chiu, W.; Bathe, M. Designer nanoscale DNA assemblies programmed from the top down. *Science* **2016**, *352* (6293), 1534.
(10) Zhan, P.; Peil, A.; Jiang, Q.; Wang, D.; Mousavi, S.; Xiong, Q.; Shen, Q.; Shang, Y.; Ding, B.; Lin, C.; et al. Recent Advances in DNA Origami-Engineered Nanomaterials and Applications. *Chem. Rev.* **2023**, *123* (7), 3976−4050.
(11) Dai, X.; Li, Q.; Aldalbahi, A.; Wang, L.; Fan, C.; Liu, X. DNA-Based Fabrication for Nanoelectronics. *Nano Lett.* **2020**, *20* (8), 5604−5615.
(12) Martynenko, I. V.; Ruider, V.; Dass, M.; Liedl, T.; Nickels, P. C. DNA Origami Meets Bottom-Up Nanopatterning. *ACS Nano* **2021**, *15* (7), 10769−10774.
(13) Posnjak, G.; Yin, X.; Butler, P.; Bienek, O.; Dass, M.; Lee, S.; Sharp, I. D.; Liedl, T. Diamond-lattice photonic crystals assembled from DNA origami. *Science* **2024**, *384* (6697), 781−785.
(14) Kahn, J. S.; Gang, O. Designer Nanomaterials through Programmable Assembly. *Angew. Chem., Int. Ed.* **2022**, *61* (3), No. e202105678.
(15) Jiang, Q.; Shang, Y.; Xie, Y.; Ding, B. DNA Origami: From Molecular Folding Art to Drug Delivery Technology. *Adv. Mater.* **2024**, *36* (22), No. 2301035.
(16) Li, L.; Yin, J.; Ma, W.; Tang, L.; Zou, J.; Yang, L.; Du, T.; Zhao, Y.; Wang, L.; Yang, Z.; et al. A DNA origami device spatially controls CD95 signalling to induce immune tolerance in rheumatoid arthritis. *Nat. Mater.* **2024**, *23* (7), 993−1001.
(17) Zeng, Y. C.; Young, O. J.; Wintersinger, C. M.; Anastassacos, F. M.; MacDonald, J. I.; Isinelli, G.; Dellacherie, M. O.; Sobral, M.; Bai, H.; Graveline, A. R.; et al. Fine tuning of CpG spatial distribution with DNA origami for improved cancer vaccination. *Nat. Nanotechnol.* **2024**, *19* (7), 1055−1065.
(18) Kopperger, E.; List, J.; Madhira, S.; Rothfischer, F.; Lamb, D. C.; Simmel, F. C. A self-assembled nanoscale robotic arm controlled by electric fields. *Science* **2018**, *359* (6373), 296−300.
(19) Thubagere, A. J.; Li, W.; Johnson, R. F.; Chen, Z. B.; Doroudi, S.; Lee, Y. L.; Izatt, G.; Wittman, S.; Srinivas, N.; Woods, D.; et al. A cargo-sorting DNA robot. *Science* **2017**, *357*, 6356.
(20) Wang, J.; Li, Z.; Willner, I. Dynamic Reconfigurable DNA Nanostructures, Networks and Materials. *Angew. Chem., Int. Ed.* **2023**, *62* (18), No. e202215332.
(21) Huang, J.; Jaekel, A.; van den Boom, J.; Podlesainski, D.; Elnaggar, M.; Heuer-Jungemann, A.; Kaiser, M.; Meyer, H.; Sacca, B. A modular DNA origami nanocompartment for engineering a cell-free, protein unfolding and degradation pathway. *Nat. Nanotechnol.* **2024**, *19* (10), 1521−1531.
(22) Wassermann, L. M.; Scheckenbach, M.; Baptist, A. V.; Glembockyte, V.; Heuer-Jungemann, A. Full Site-Specific Addressability in DNA Origami-Templated Silica Nanostructures. *Adv. Mater.* **2023**, *35* (23), No. 2212024.
(23) Wagenbauer, K. F.; Wachauf, C. H.; Dietz, H. Quantifying quality in DNA self-assembly. *Nat. Commun.* **2014**, *5*, 3691.
(24) Iinuma, R.; Ke, Y.; Jungmann, R.; Schlichthaerle, T.; Woehrstein, J. B.; Yin, P. Polyhedra Self-Assembled from DNA Tripods and Characterized with 3D DNA-PAINT. *Science* **2014**, *344* (6179), 65−69.
(25) van Wee, R.; Filius, M.; Joo, C. Completing the canvas: advances and challenges for DNA-PAINT super-resolution imaging. *Trends Biochem. Sci.* **2021**, *46* (11), 918−930.
(26) Strauss, M. T.; Schueder, F.; Haas, D.; Nickels, P. C.; Jungmann, R. Quantifying absolute addressability in DNA origami with molecular resolution. *Nat. Commun.* **2018**, *9* (1), 1600.
(27) Green, C. M.; Hughes, W. L.; Graugnard, E.; Kuang, W. Correlative Super-Resolution and Atomic Force Microscopy of DNA Nanostructures and Characterization of Addressable Site Defects. *ACS Nano* **2021**, *15* (7), 11597−11606.
(28) Eklund, A. S.; Comberlato, A.; Parish, I. A.; Jungmann, R.; Bastings, M. M. C. Quantification of Strand Accessibility in Biostable DNA Origami with Single-Staple Resolution. *ACS Nano* **2021**, *15* (11), 17668−17677.
(29) Douglas, S. M.; Dietz, H.; Liedl, T.; Högberg, B.; Graf, F.; Shih, W. M. Self-assembly of DNA into nanoscale three-dimensional shapes. *Nature* **2009**, *459* (7245), 414−418.
(30) Lee, C.; Kim, K. S.; Kim, Y. J.; Lee, J. Y.; Kim, D. N. Tailoring the Mechanical Stiffness of DNA Nanostructures Using Engineered Defects. *ACS Nano* **2019**, *13* (7), 8329−8336.
(31) Scheckenbach, M.; Schubert, T.; Forthmann, C.; Glembockyte, V.; Tinnefeld, P. Self-Regeneration and Self-Healing in DNA Origami Nanostructures. *Angew. Chem., Int. Ed.* **2021**, *60* (9), 4931−4938.
(32) Douglas, S. M.; Marblestone, A. H.; Teerapittayanon, S.; Vazquez, A.; Church, G. M.; Shih, W. M. Rapid prototyping of 3D DNA-origami shapes with caDNAno. *Nucleic Acids Res.* **2009**, *37* (15), 5001−5006.

https://doi.org/10.1021/jacsau.5c00206
JACS Au 2025, 5, 2237−2245

(33) Wade, O. K.; Woehrstein, J. B.; Nickels, P. C.; Strauss, S.; Stehr, F.; Stein, J.; Schueder, F.; Strauss, M. T.; Ganji, M.; Schnitzbauer, J.; et al. 124-Color Super-resolution Imaging by Engineering DNA-PAINT Blinking Kinetics. *Nano Lett.* **2019**, *19* (4), 2641−2646.
(34) Schueder, F.; Stein, J.; Stehr, F.; Auer, A.; Sperl, B.; Strauss, M. T.; Schwille, P.; Jungmann, R. An order of magnitude faster DNA-PAINT imaging by optimized sequence design and buffer conditions. *Nat. Methods* **2019**, *16* (11), 1101−1104.
(35) Jungmann, R.; Steinhauer, C.; Scheible, M.; Kuzyk, A.; Tinnefeld, P.; Simmel, F. C. Single-Molecule Kinetics and Super-Resolution Microscopy by Fluorescence Imaging of Transient Binding on DNA Origami. *Nano Lett.* **2010**, *10* (11), 4756−4761.

https://doi.org/10.1021/jacsau.5c00206
JACS Au 2025, 5, 2237−2245